EASR

Engineering and Applied Science Research

https://www.tci-thaijo.org/index.php/easr/index

Published by the Faculty of Engineering, Khon Kaen University, Thailand

Superior mechanical and tribological properties of Al7075 metal matrix nanocomposites processed through a novel multi-stage casting route

Charinrat Potisawang, Kowit Ponhan and Sukangkana Talangkun*

Department of Industrial Engineering, Faculty of Engineering, Khon Kaen University, Khon Kaen 40002, Thailand

Received 21 April 2025
Revised 2 July 2025
Accepted 5 August 2025

Abstract

This study aims to improve the microstructural features and mechanical performance of Al7075 aluminium matrix composites reinforced with silicon carbide (SiC) nanoparticles and graphite (Gr) through a novel processing route. The proposed method integrates mechanical alloying-assisted semisolid stir casting with die casting, followed by a T6 heat treatment. The Al7075/SiC composite subjected to T6 treatment exhibited superior mechanical properties, including a microhardness of 218 HV, a 0.2% proof stress of 250 MPa, an ultimate tensile strength of 364 MPa, and an elongation of 16%. These enhancements are primarily attributed to synergistic strengthening mechanisms, including grain refinement, Orowan looping, and precipitation hardening. In contrast, the Al7075/SiC/Gr hybrid composite demonstrated a marginally reduced ultimate tensile strength of 254 MPa, representing a 12% decline compared to the Al7075/SiC composite, which was attributed to graphite agglomeration and inadequate interfacial bonding. Wear resistance testing revealed that the SiC-reinforced composite exhibited the lowest material loss, with scanning electron microscopy (SEM) analyses confirming reduced groove depth and plastic deformation. Conversely, the hybrid composite displayed increased surface roughness and porosity, primarily due to graphite-induced defects. These findings indicate that the incorporation of SiC nanoparticles, in conjunction with T6 heat treatment, constitutes an effective strategy for enhancing the structural integrity and mechanical performance of Al7075-based composites. However, further optimization of graphite morphology and dispersion is necessary to fully realize its potential as a solid lubricant in hybrid composite systems.

Keywords: Al7075 Nanocomposite, SiC Nanoparticles, T6 Heat treatment, Mechanical properties

1. Introduction

The Al7075 aluminium alloy is extensively utilized in the aerospace and automotive sectors as a result of its superior strength-to-weight ratio, favorable ductility, low density, and exceptional resistance to fatigue loading [1]. Die casting (DC) has emerged as a highly efficient near-net-shape manufacturing process, enabling the fabrication of intricate, lightweight components with high dimensional precision. The inherent characteristics of the die casting process, notably its rapid solidification rates and high injection speeds, facilitate the development of ultra-fine grain structures. This microstructural refinement contributes to enhanced mechanical performance of Al7075 alloys relative to their coarse-grained counterparts subjected to equivalent heat treatment conditions [2, 3]. Despite the aforementioned advantages, the presence of coarse secondary phases, such as AlZnMgCu and Al_2CuMg, along with the segregation of alloying elements at grain boundaries, imposes significant constraints on the mechanical performance of Al7075 alloy [4]. Additionally, the formation of iron-rich and silicon-based intermetallic compounds further exacerbates crack initiation and propagation, thereby undermining the structural integrity of the material [5].

The incorporation of ceramic reinforcements, particularly silicon carbide (SiC), has been shown to markedly enhance the mechanical properties of Al7075-based composites. Microstructural characterization reveals that the addition of SiC promotes the formation of more spheroidal α-Al grains and modifies the morphology of intermetallic phases into shorter, plate-like structures, thereby resulting in a more refined and homogeneous microstructure [6]. The presence of SiC particles within the fracture surfaces further suggests an effective load transfer mechanism, wherein the applied tensile stress is efficiently transmitted from the relatively ductile aluminium matrix to the stiffer ceramic reinforcements, leading to improved tensile strength. This enhancement underscores the potential of metal matrix composites (MMCs) as advanced structural materials for demanding engineering applications [7]. Despite recent advancements, the fabrication of aluminium matrix nanocomposites continues to present significant challenges, particularly in achieving a consistent dispersion of nanoparticles inside the molten aluminium matrix. These difficulties primarily arise from the poor wettability and inherently high surface-to-volume ratio of ceramic nanoparticles. Such factors often promote agglomeration and clustering of nanoparticles, which adversely affect microstructural homogeneity and significantly undermine the mechanical integrity and overall performance of the resulting composites [8].

Ensuring uniform dispersion of nanoparticles throughout the aluminium matrix continues to be a significant obstacle in the production of aluminium matrix composites (AMCs). Among various manufacturing techniques, stir casting is widely employed due to its operational simplicity, cost-effectiveness, and scalability for industrial production [9]. Nevertheless, conventional stir casting often falls short in ensuring uniform nanoparticle dispersion, primarily due to limitations such as poor wettability, particle

*Corresponding author.
Email address: sukangkana@kku.ac.th
doi: 10.14456/easr.2025.51

agglomeration, and clustering [10]. Mechanical alloying (MA) has been recognized as a promising solid-state pre-processing method to address these limitations. It employs high-energy ball milling to subject powder particles to repetitive cycles of cold welding and fragmentation, which enhances the identical integration of reinforcing particles in the aluminium matrix [11, 12]. Recent investigations have shown that pre-mixing aluminium powders with nanoscale reinforcements via MA prior to stir casting significantly improves the particle dispersion in the molten alloy [13]. Furthermore, Ponhan et al. [14] demonstrated that compacting the mechanically alloyed ADC12/SiC composite powders into pellets before their introduction into the molten aluminium enhances compositional uniformity and promotes improved integration of the reinforcement during casting. This hybrid approach ensures more uniform dispersion before solidification and contributes to a refined and consistent microstructure.

To enhance the microstructural features and mechanical performance of Al7075-based aluminium matrix nanocomposites for advanced engineering applications, this study proposes a novel fabrication approach that integrates semisolid stir casting assisted by master pellet feeding with the die casting process. This hybrid technique facilitates the even dispersion of nanoparticles in the aluminium matrix, while simultaneously refining both the matrix microstructure and intermetallic phase morphology, thereby contributing to improved strengthening mechanisms. Furthermore, the fabricated Al7075/SiC nanocomposites were subjected to T6 heat treatment to promote precipitation strengthening, leading to further enhancement in mechanical properties [15]. This combined processing strategy has not been previously reported in the literature. In addition, the present study systematically investigates the influence of SiC reinforcement and processing parameters on the microstructure, tensile behavior, and wear resistance of the developed composites.

2. Materials and methods

2.1 Material selection

Al7075 alloy was employed as the matrix material, while silicon carbide (SiC) nanoparticles and graphite (Gr) were selected as reinforcing agents. The chemical composition of the Al7075 alloy was determined using an ARL 3460 OE Spectrometer, (Thermo Fisher Scientific, Waltham, MA, USA), and the results are presented in Table 1. The Al7075 powder was prepared via a CNC milling machine (Computer Numerical Control milling machine), followed by a grinding process to achieve finer particle sizes. Figure 1 illustrates the morphological features of the starting powders of Al7075, SiC, and Gr. As shown in Figure 1(a), the Al7075 powder possessed a flake-like morphology with an average particle size close to 200 µm. The SiC nanoparticles, shown in Figure 1(b), displayed a spherical morphology with an average particle size of 50 nm and exhibited a tendency toward agglomeration in the initial state. The graphite powder, as depicted in Figure 1(c), also possessed a flake-like structure with a mean particle size of 74 µm.

Table 1 Chemical constituents of Al7075 alloy (wt.%).

Elements	Weight %							
	Zn	**Mg**	**Cu**	**Cr**	**Fe**	**Si**	**Mn**	**Al**
Std. 7075	5.5-6.1	2.1-2.9	1.2-2.0	0.18-0.28	0.5max	0.4 max	0.3 max	Balance
As received	5.43	2.5	1.21	0.25	0.13	0.04	0.04	Balance

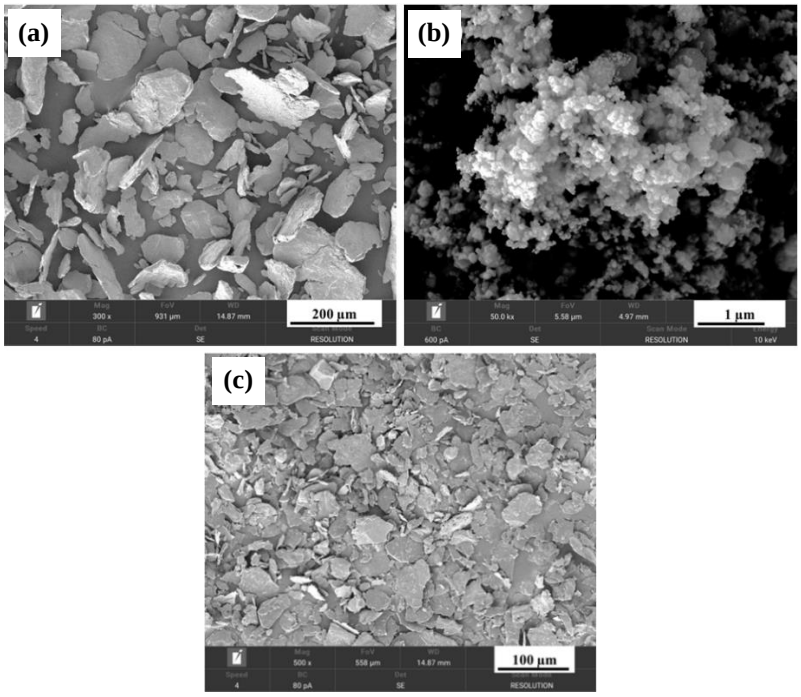

Figure 1 Representative SEM illustrations of initial materials: (a) Al7075 powder (b) nano-sized SiC particles (c) micron-sized graphite powder.

Furthermore, the relationship between liquid fraction and temperature for the Al7075 aluminium ingot was investigated using Differential Scanning Calorimetry (DSC), performed with a HITACHI DSC 7020 instrument (Hitachi High-Tech Science Corporation, Tokyo, Japan). A sample weighing approximately 6 mg was introduced in an alumina crucible, then subjected to heating at a rate of

10 °C/min up to 700 °C under a nitrogen atmosphere. The resulting correlation between temperature and liquid fraction is depicted in Figure 2. The analysis revealed that the melting range of the Al7075 ingot spans from 489.9 °C to 640 °C. Therefore, the semi-solid stir casting was performed at 630 °C in this study, corresponding to approximately 70% liquid fraction

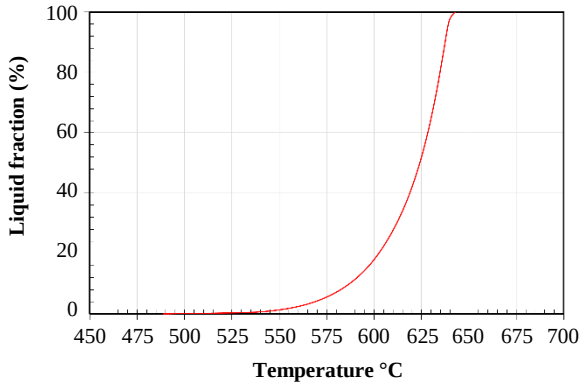

Figure 2 Relationship of liquid phase fractions and temperature of Al7075 alloy examined by Differential Scanning Calorimetry (DSC).

2.2 Fabrication process of Al7075 aluminium nanocomposites

In the initial stage of the fabrication process, composite master pellets were synthesized through mechanical alloying (MA) followed by cold compaction. Two types of master pellets were prepared: the first consisted of Al7075 powder reinforced with nano-sized SiC particulates in a mass ratio of 20:2, referred to as the Al7075/SiC composite. The second type, designated as the Al7075/SiC/Gr composite, comprised Al7075 powder, SiC nanoparticles, and graphite (Gr) powder in a mass ratio of 20:2:1. For both mixtures, mechanical alloying was performed in a planetary ball mill using a 480 mL stainless-steel container, with a ball-to-powder weight ratio of 10:1. To minimize excessive cold welding, 1 wt.% stearic acid was added as a process control agent. A total of 575 stainless steel balls (10 mm diameter, 4 g each) were used. Milling was conducted for 20 hours at a constant rotational speed of 150 rpm, with 20-minute cooling intervals to prevent overheating. The resulting powders were compacted uniaxially at a pressure of 150 MPa at ambient temperature to form cylindrical master pellets.

In the second stage, the semi-solid stir casting was employed. A 200 g Al7075 ingot was melted in a silicon carbide crucible at 650 °C under an argon atmosphere. The molten alloy was mechanically agitated at 300 rpm for 5 minutes, during which a commercial flux (Clover All-11) was added to eliminate impurities. The pre-fabricated composite master pellets were heated to 200 °C for 5 minutes prior to being introduced into the Al7075 melt at 680 °C. Manual stirring was applied to ensure entire dissolution of the pellets into the molten alloy. Subsequently, the temperature was lowered to 630 °C, corresponding to approximately 70% liquid fraction, as determined from the DSC analysis presented in Figure 2, to induce a semi-solid condition. The slurry was then stirred for an additional 10 minutes using a stainless-steel impeller to promote uniform dispersion of SiC reinforcements. Subsequently, the temperature of the molten alloy was raised to 650 °C, and the composite melt was cast into a die preheated to 200 °C to form rod-shaped specimens measuring 16 × 15.6 × 205 mm, utilizing a 125-ton cold chamber die casting machine (Model BD-125V4-T, Toyo Machinery & Metal Co., Ltd., Tokyo, Japan). The injection speed and pressure were set at 3 m/s and 11 MPa, respectively. The specimens were subsequently subjected to T6 heat treatment, comprising solutionizing at 480 °C for 1 hour as suggested by Walde et al. [16] , followed by quenching in water and artificial aging at 135 °C for 20 hours to achieve peak age. For comparison, an unreinforced Al7075 alloy sample was fabricated using the same processing parameters. The novel multi-stage casting route developed in this study is represented in Figure 3.

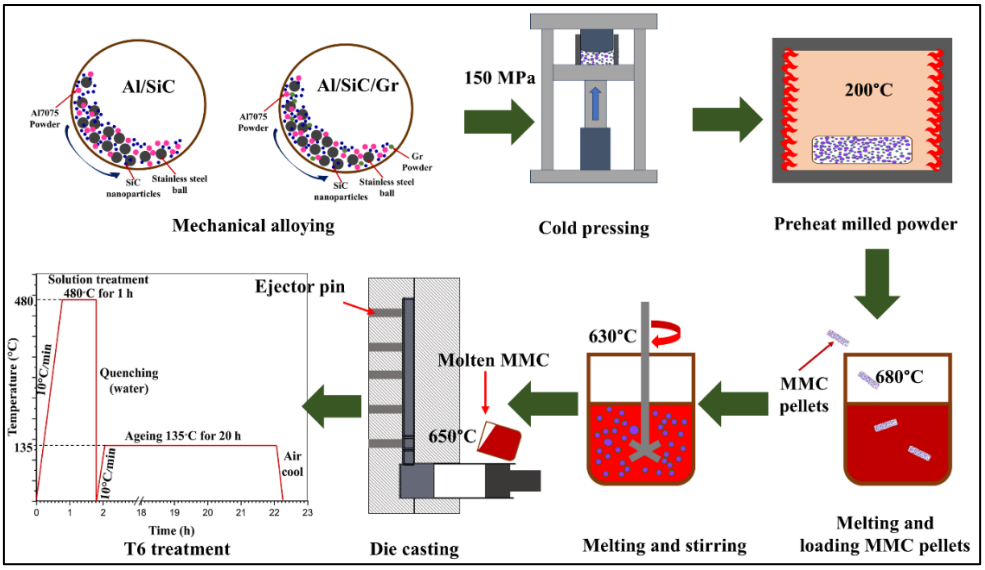

Figure 3 Schematics illustration for the novel fabrication process involving semi-solid stir casting, followed by die casting and T6 heat treatment.

2.3 Microstructural characterization

The manufactured specimens were initially subjected to grinding using silicon carbide abrasive papers with progressively finer grit sizes, ranging from P320 to P1000. This was followed by polishing with 9 μm and 3 μm diamond suspensions, as well as a final polish was accomplished using 0.1 μm SiO_2 paste. Afterwards, the polished specimens were then etched at room temperature for 10 seconds using an etchant composed of 25 ml each of hydrochloric acid, nitric acid, and methanol, along with one drop of hydrofluoric acid. Microstructural analysis was carried out using an optical microscope (Olympus BX60) and a field emission scanning electron microscope (FE-SEM, TESCAN MIRA) equipped with an energy-dispersive spectroscopy (EDS) system. Samples for SEM images were taken from the cross-section in the longitudinal direction of flow of the cast specimens.

2.4 Physical and mechanical property investigation

The microhardness of the polished specimens was evaluated via a Wilson Vickers hardness tester under a 100-gf load and a dwell time of 15 seconds. Each reported microhardness value represents the average of sixteen indentations taken from different regions of the alloy or composite specimens to ensure statistical reliability. For tensile testing, the die-cast products were machined into standard dumbbell-shaped specimens in accordance with ASTM E8 specifications, featuring a gauge length of 36 mm, a diameter of 9 mm, and a fillet radius of 8 mm. Tensile testing was conducted with a universal testing machine (Shimadzu, Model: EHF-EG10-20L, Japan) operating at a fixed crosshead speed of 0.50 mm/min at room temperature. The load–displacement data collected during testing were utilized to generate stress–strain curves for assessing the tensile behavior. For each sample type, the 0.2% proof stress, tensile strength, and elongation percentage were computed as the average of three separate measurements to ensure reproducibility. Additionally, the tribological behavior of the fabricated samples was evaluated using a ball-on-disc tribometer (CSM Instruments), where each sample was mounted horizontally on the rotating disc. A tungsten carbide (WC) ball with a diameter of 6 mm was used as the counter face. Before testing, the specimens and the WC ball were subjected to ultrasonic cleaning in acetone for 10 minutes, followed by drying with hot air. The wear experiments were conducted under a 5 N normal load, at a sliding speed of 16 cm/s, and over a total distance of 500 meters. Weight loss was determined by measuring the mass of each specimen before and after testing using a precision electronic balance with a sensitivity of 0.1 mg. Each wear test condition was repeated at least three times, and the average value was reported. Also, theoretical densities of the samples were calculated using the rule of mixtures, while actual densities were measured with an electronic densimeter (Model MD-300S). For all density measurements, a minimum of three readings were taken per sample to ensure reproducibility.

3. Results and discussion

3.1 Microstructural investigation

Figure 4 displays the microstructural features of the as-cast Al7075 alloy fabricated via the die casting process. As indicated in Figure 4(a), the microstructure was primarily composed of coarse rosette-shaped α-Al grains, surrounded by needle-like intermetallic phases of varying sizes. These intermetallic phases, predominantly located along the grain boundaries, were identified as Mg $(Zn,Cu,Al)_2$, Al_2Cu, Al_7Cu_2Fe, and Mg_2Si. The fundamental components of the individual phases, as examined by EDS, are presented in Figure 4(b).

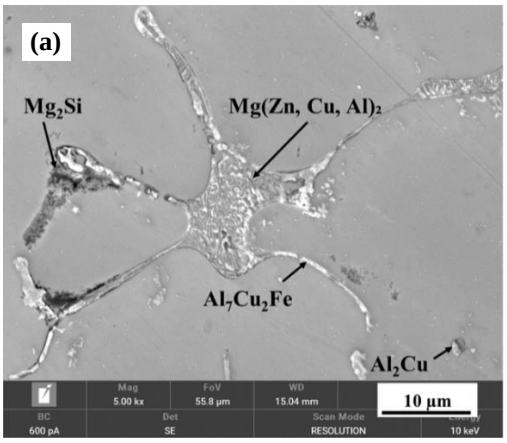

(b)

Possible phase	Element (atomic %)						
	Al	Zn	Mg	Cu	Fe	Si	C
Mg (Zn, Cu, Al)$_2$	30.31	20.26	24.16	25.27	-	-	-
Al_7Cu_2Fe	77.59	-	-	5.59	16.82	-	-
Al_2Cu	35.13	2.89	2.4	15.59	4.3	2.9	36.79
Mg_2Si	35.72	0.2	36.73	0.06	-	27.29	-

Figure 4 SEM image of as-cast Al7075 and EDS analysis of possible phase found at grain boundaries.

Figure 5 provides a comparative overview of the microstructural features observed in the three different fabricated materials. As illustrated in Figure 5(a), the microstructure of the unreinforced Al7075 alloy displayed coarse rosette-shaped α-Al grains surrounded by elongated, needle-like intermetallic phases. In contrast, the Al7075/SiC composite, presented in Figure 5(b), demonstrated a more refined microstructure characterized by spheroidized α-Al grains and shorter, plate-like intermetallic formations. This microstructural refinement is primarily attributed to the introduction of SiC nanoparticles, which serve as efficient heterogeneous nucleation positions and inhibit the growth of both α-Al grains and intermetallic phases during solidification [17, 18]. The localized distribution of SiC is attributed to its role as a heterogeneous nucleation site and its poor wettability with the Al matrix, resulting in clustering at specific locations during solidification. In Figure 5(c), the Al7075/SiC/Gr hybrid composite shows a different microstructural evolution. The addition of graphite resulted in its segregation along the grain boundaries, accompanied by a coarser and less uniform distribution of α-Al grains and intermetallic phases when compared to the SiC-reinforced composite. This behavior is ascribed to the inherent

characteristics of graphite, which acts as both a solid lubricant and a nucleation inhibitor due to its poor wettability and low interfacial energy with the aluminium matrix. As a result, the number of effective nucleation sites is reduced during solidification, allowing grains to grow larger. Moreover, the non-wetting nature of graphite causes it to segregate at the grain boundaries, where it promotes the accumulation of alloying elements and the formation of coarse intermetallic phases. Figure 5(d) quantitatively supports these observations by comparing the average grain sizes of the three materials. The Al7075/SiC composite exhibited the smallest average grain size, confirming the grain-refining effect of SiC nanoparticles. In contrast, the Al7075/SiC/Gr hybrid composite showed a notable increase in grain size due to the adverse influence of graphite on nucleation and solidification behavior. It is worth noting that processing conditions also significantly influence grain size. For instance, Dong et al. [19] found that adding TiB_2 nanoparticles during die casting reduced the α-Al grain size by approximately 60%, leading to a refined structure and improved mechanical properties. Critical factors in die-cast composites include porosity, solidification rate, and dispersibility.

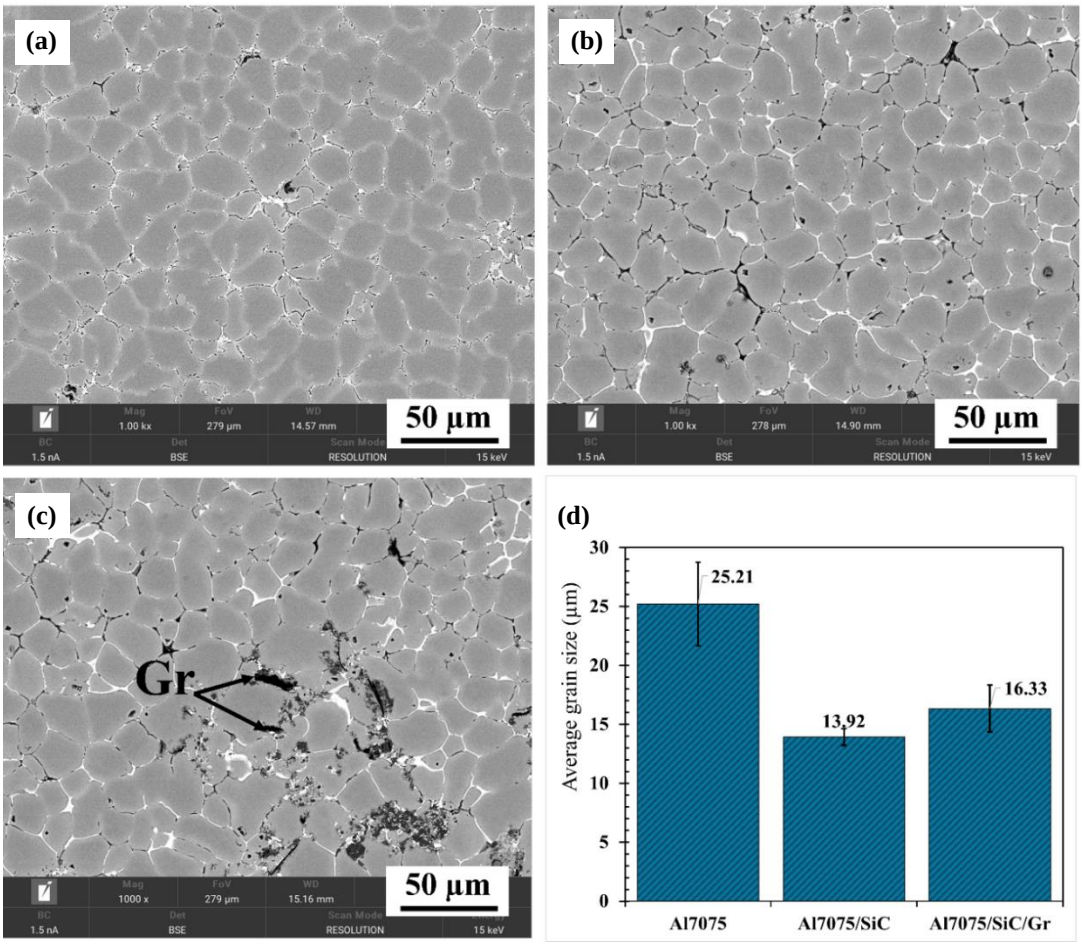

Figure 5 Representative SEM micrographs of the cross section in longitudinal direction (a) Al7075 alloy, (b) Al7075/SiC, and (c) Al7075/SiC/Gr composites fabricated via a cold chamber die casting, and (d) Comparison of average grain sizes.

Figure 6 illustrates the microstructural characteristics of three types of fabricated materials subjected to T6 heat treatment. In the case of the as-cast Al7075 alloy without T6 treatment, shown in Figure 6(a), the microstructure revealed prominent α-Al grains surrounded by thick, continuous intermetallic phases located along the grain boundaries. EDS mapping confirmed the occurrence of main alloying elements, including Zn, Cu, Fe, Mg, Si, and C, which contributed to the development of these intermetallic compounds. Following T6 heat treatment, as shown in Figure 6(b), the intermetallic phases became more refined and exhibited a discontinuous distribution along the grain boundaries. This transformation is primarily due to the high-temperature solution treatment, which dissolves the coarse and continuous intermetallic phases present in the as-cast microstructure. Upon rapid quenching, the dissolved alloying elements, primarily Zn, Mg, and Cu, are retained within the aluminium matrix, forming a supersaturated solid solution. Subsequent artificial aging induces the precipitation of fine, coherent phases both within the grains and along the grain boundaries, resulting in a more refined and dispersed microstructure compared to the untreated condition [20]. EDS mapping further confirmed the formation of these precipitates; however, some elemental agglomeration was still observed, indicating a degree of non-uniformity in elemental distribution post-treatment. Figure 6(c) presents the microstructure of the Al7075/SiC composite after T6 treatment, showing a more uniform distribution of the refined, discontinuous, plate-like intermetallic phases. EDS analysis confirmed a more homogeneous dispersion of alloying elements throughout the matrix, indicating improved microstructural stability. In Figure 6(d), the Al7075/SiC/Gr hybrid composite exhibited the presence of carbon-rich regions, with slight clustering of graphite (Gr) particles along the grain boundaries. The detection of these C-rich zones confirms the presence of graphite flakes. Notably, the T6 treatment did not alter the morphology or distribution of the Gr clusters, as they remained undissolved and retained their flake-like structure at the grain boundaries.

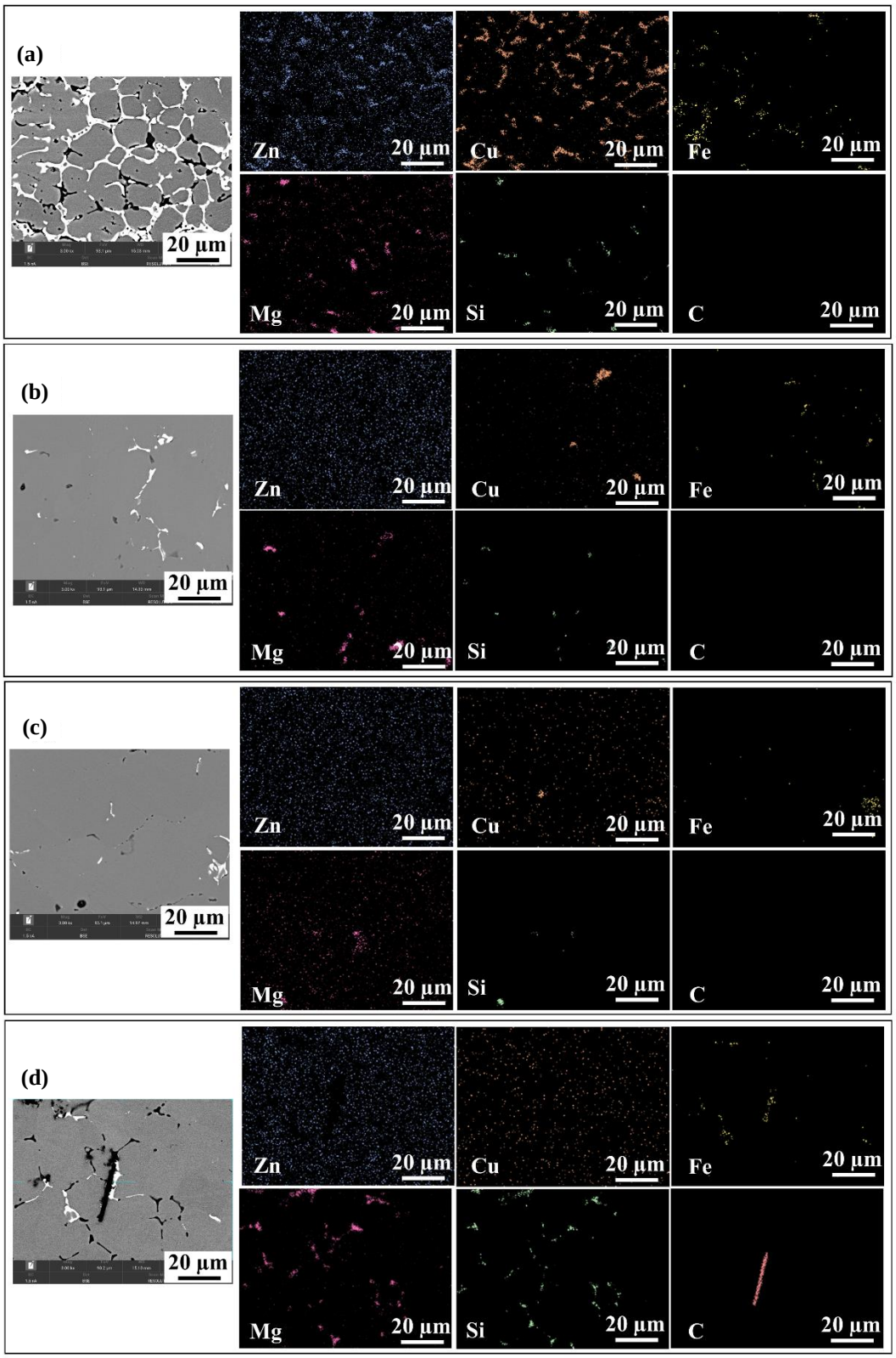

Figure 6 SEM micrographs equipped with and EDS mapping analysis of (a-b) Al7075 in as-cast and T6 conditions, (c) Al7075/SiC in T6 treated conditions and (b) Al7075/SiC/Gr in T6 treated conditions.

3.2 Property examination

3.2.1 Density and porosity

The relative density and porosity values of Al7075 and its composites are provided in Table 2. The unreinforced Al7075 alloy demonstrated a porosity level of 0.036%, while the Al7075/SiC composite demonstrated the lowest porosity at 0.018%. In contrast, the Al7075/SiC/Gr hybrid composite showed the highest porosity, measured at 0.542%. This increase is primarily attributed to the poor wettability between graphite and the aluminium matrix, as well as graphite's propensity to entrap gases during the fabrication process.

Due to the lack of strong interfacial bonding with molten aluminium, graphite particles tend to form voids at the particle matrix interface. Additionally, the agglomeration of graphite particles in the melt can lead to the formation of clusters, which may serve porosity [21]. These findings are consistent with the microstructural observations presented in Figure 5 (c).

Table 2 Density and porosity of Al7075 and composite after T6 heat treatment

Materials	Density (g/cm^3)		Relative Density (%)	Porosity (%)
	Theoretical	Experimental		
Al7075	2.800	2.799±0.004	99.964	0.036
Al7075/SiC	2.814	2.813±0.002	99.982	0.018
Al7075/SiC/Gr	2.816	2.801±0.002	99.458	0.542

3.2.2 Microhardness

Figure 7 presents the average microhardness values of all samples under both as-cast and T6 heat-treated conditions. The results indicated a significant improvement in hardness for the composites compared to the base Al7075 alloy. The as-cast Al7075 alloy exhibited an average microhardness of 125 HV. The addition of nanoscale SiC particulates into the Al7075 alloy led to a notable increase of 14.8%, achieving a hardness of 144 HV. This improvement in hardness can be primarily attributed to multiple strengthening mechanisms. Firstly, the SiC nanoparticles dispersed within the aluminium matrix serve as effective obstructions to dislocation motion during indentation, thus increasing resistance to plastic deformation [22]. Additionally, the presence of SiC particles promotes the refinement of primary α-Al grains, resulting in a higher grain boundary density. These grain boundaries further inhibit dislocation movement, contributing to the observed hardness improvement [23]. In comparison, the Al7075/SiC/Gr hybrid composite exhibited a moderate increase in hardness, with an 8.4% improvement over the base alloy, reaching 136 HV. This relatively lower enhancement is ascribed to the non-uniform grain size and the clustering of graphite particles at the grain boundaries, which may reduce the effectiveness of load transfer and reinforcement.

Following T6 heat treatment, all samples demonstrated a substantial increase in hardness. The heat-treated Al7075 alloy reached a hardness of 178 HV, representing a 42.4% increase compared to its as-cast counterpart. This improvement is attributed to microstructural refinement and the precipitation strengthening mechanism activated during aging. The Al7075/SiC and Al7075/SiC/Gr composites achieved even greater hardness values of 218 HV and 194 HV, corresponding to increases of 51.38% and 42.64%, respectively, over the untreated Al7075 alloy. The pronounced enhancement in hardness for the SiC-reinforced composite is largely due to the increased formation of fine precipitates around the SiC nanoparticles, which act as barrier for dislocation movement during. According to Pu et al. [24], the precipitation behavior in Al7075/SiC composites differs from that of the monolithic Al7075 alloy after T6 treatment. Even a small addition of 1 vol.% SiC can significantly influence the morphology and distribution of precipitates, resulting in a more uniform and finely dispersed precipitate structure that contributes to superior mechanical properties.

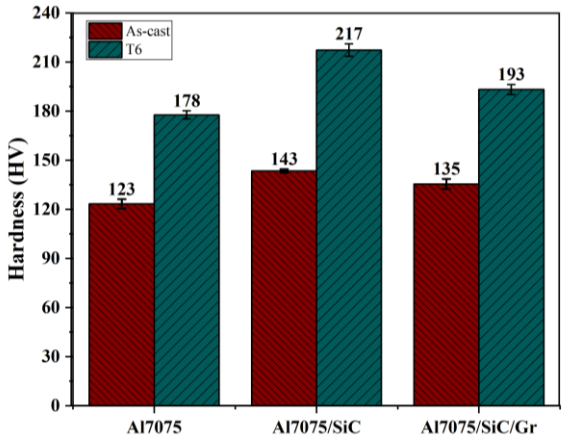

Figure 7 Representative microhardness of Al7075, Al7075/SiC, Al7075/SiC/Gr under as-cast and T6 heat treatment conditions.

3.2.3 Tensile properties

Figure 8(a) illustrates the tensile stress–strain curves of Al7075 and its composites for as-cast and T6 conditions. Adding nanoscale SiC particles extensively persuaded the deformation behavior of the fabricated composites. The unreinforced Al7075 alloy exhibited the lowest slope in the initial linear region of the stress–strain curve, indicating the lowest elastic modulus among the tested samples. In contrast, the Al7075/SiC composite displayed the steepest slope, reflecting the highest elastic modulus. This enhancement in stiffness is attributed to the uniform and dense dispersion of nano-sized SiC particles in the α-Al matrix, which restricts dislocation motion due to the inherent high stiffness and fracture strength of the reinforcement phase. The α-Al matrix effectively transfers the applied load to the SiC particles during tensile deformation, thereby improving the composite's elastic response [14]. Moreover, following T6 heat treatment, an increase in the slope of the linear region was observed for all samples, signifying a further enhancement in elastic modulus. This improvement is primarily due to precipitation strengthening, where the formation of fine, coherent precipitates within the matrix contributes to increased resistance to dislocation movement and thus improved mechanical performance [25].

The detailed tensile properties of the investigated materials are presented in Figure 8(b). The as-cast Al7075 alloy exhibited a 0.2% proof stress of 90 MPa, an ultimate tensile strength (UTS) of 205 MPa, and an elongation of 7%. Notably, the Al7075 composite reinforced with 1.0 wt.% SiC nanoparticles demonstrated significantly enhanced mechanical performance, with corresponding values of 190 MPa for 0.2% proof stress, 290 MPa for UTS, and 8% elongation. The improvement in tensile properties of the Al7075/SiC

composite can be attributed to several concurrent strengthening mechanisms. First, grain refinement is achieved through the heterogeneous nucleation of α-Al grains by the SiC nanoparticles, resulting in a finer microstructure that impedes dislocation motion and enhances strength. Second, dislocation strengthening occurs due to the generation of geometrically necessary dislocations arising from the mismatch in the coefficient of thermal expansion (CTE) between the SiC reinforcements and the Al7075 matrix. Third, Orowan strengthening contributes to the overall enhancement, as dislocations are hindered by the presence of finely dispersed SiC nanoparticles, increasing the energy barrier for dislocation motion. In addition, during tensile loading, the applied stress is effectively transferred from the ductile Al7075 matrix to the stiffer SiC particles, improving the load-bearing capacity of the composite [26, 27]. In contrast, the inclusion of brittle graphite (Gr) flakes in the Al7075/SiC/Gr hybrid composite led to a slight reduction in tensile performance. The UTS decreased to 254 MPa, representing a 12% decline compared to the Al7075/SiC composite. This decrease is primarily attributed to the presence of micro-clusters of Gr particles at the grain boundaries, which act as stress concentrators and promote premature failure under tensile loading. Moreover, the tensile performance of all manufactured samples was notably improved following T6 heat treatment. For instance, the 0.2% proof stress, ultimate tensile strength (UTS), and elongation of the Al7075 alloy increased by 167%, 41%, and 86%, respectively, compared to the as-cast condition. Among all the materials studied, the Al7075/SiC-T6 nanocomposite exhibited the most superior tensile performance, achieving a 0.2% proof stress of 250 MPa, a UTS of 364 MPa, and an elongation of 16%. These enhancements are primarily attributed to the effects of the T6 heat treatment process, which comprises solution treatment, quenching, and artificial aging. During this process, the aluminium matrix undergoes precipitation hardening, predominantly through the formation of finely dispersed η' ($MgZn_2$) precipitates. These nanoscale precipitates act as effective barriers to dislocation motion, thereby significantly increasing the tensile strength of the alloy [28]. The observed improvements in the Al7075/SiC nanocomposite can thus be ascribed to the synergistic effect of precipitation hardening in the matrix and dispersion strengthening provided by the uniformly distributed SiC nanoparticles. Together, these mechanisms result in the remarkable enhancement in the mechanical performance of the composite materials following T6 treatment [29].

It is important to note that fabrication method significantly affects the mechanical properties of composites. Canakci et al. [30] investigated composites fabricated by stir casting and found that fractures often occurred at reinforcement agglomeration sites. They also reported difficulties in controlling defects such as pores and clusters during the stir casting process. In contrast, Guo et al. [31] reported that rheo-die cast samples exhibited extremely low porosity and a fine, uniform microstructure throughout the casting, leading to significantly improved strength and ductility in the as-cast condition. In this investigation, the mechanical properties are improved through the reduction of porosity and the uniform distribution of the nano-particle reinforcement phase through the combination of mechanical alloying and die casting.

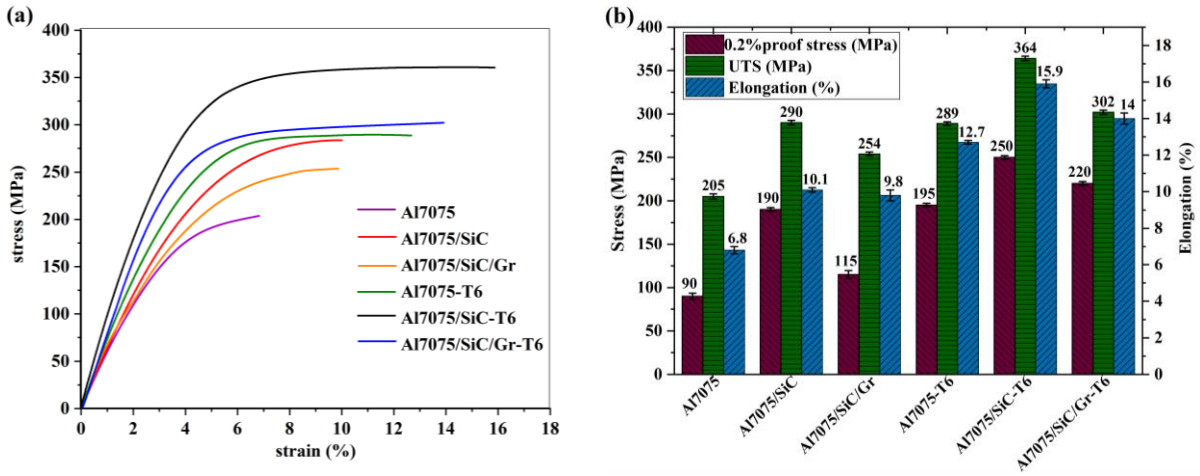

Figure 8 (a) Engineering stress-strain curve for all fabricated samples for as-cast and T6 conditions and (b) Representative tensile properties for all samples.

Figure 9 presents the tensile fracture surfaces of the produced specimens following T6 heat treatment. As depicted in Figure 9(a), the unreinforced Al7075 alloy presented prominent cleavage fractures within the α-Al grains and the presence of long, thick tearing edges of intermetallic phases distributed along the grain boundaries. In contrast, the fracture surface of the Al7075/SiC composite, shown in Figure 9(b), revealed a more refined morphology characterized by short and narrow tearing ridges, small quasi-cleavage planes, and increased number of dimples interspersed among the ridges. Additionally, SiC particles were visibly embedded within the fractured surface, indicating an effective load transfer mechanism wherein the applied tensile load is transmitted from the relatively soft aluminium matrix to the stiffer ceramic reinforcement, thereby enhancing the tensile strength of the composite [32]. EDS analysis of the fracture surface (Point A) detected the presence of Si along with Mg, Zn, and Cu, suggesting the formation of precipitated phases in proximity to the SiC particles. In Al–Zn–Mg–Cu alloys, the Cu-rich Guinier–Preston (GP) zones gradually evolve into the strengthening $MgZn_2$ phase during the aging process. According to the study by Shi et al. [9], EDS mapping revealed the enrichment of Mg, Zn, Cu, and O elements around the SiC particles. These findings suggest that the introduction of SiC facilitates localized enrichment of alloying elements, thereby accelerating the transformation of GP zones into the $MgZn_2$ phase, contributing to the overall strengthening of the composite. The fracture morphology of the Al7075/SiC/Gr hybrid composite, illustrated in Figure 9(c), was generally comparable to that of the Al7075/SiC composite. However, additional features were observed, including graphite layers aligned along the grain boundaries. These layers contributed to void formation and acted as sites for crack initiation and propagation, which ultimately led to a reduction in the composite's tensile properties. EDS analysis at a representative point (Point B) confirmed a high concentration of carbon, verifying the presence of graphite. While the SiC particles continued to provide reinforcement, the layered graphite structure facilitated crack propagation and embrittlement, resulting in a mixed-mode fracture behavior characterized by both strengthening and fracture-initiating features.

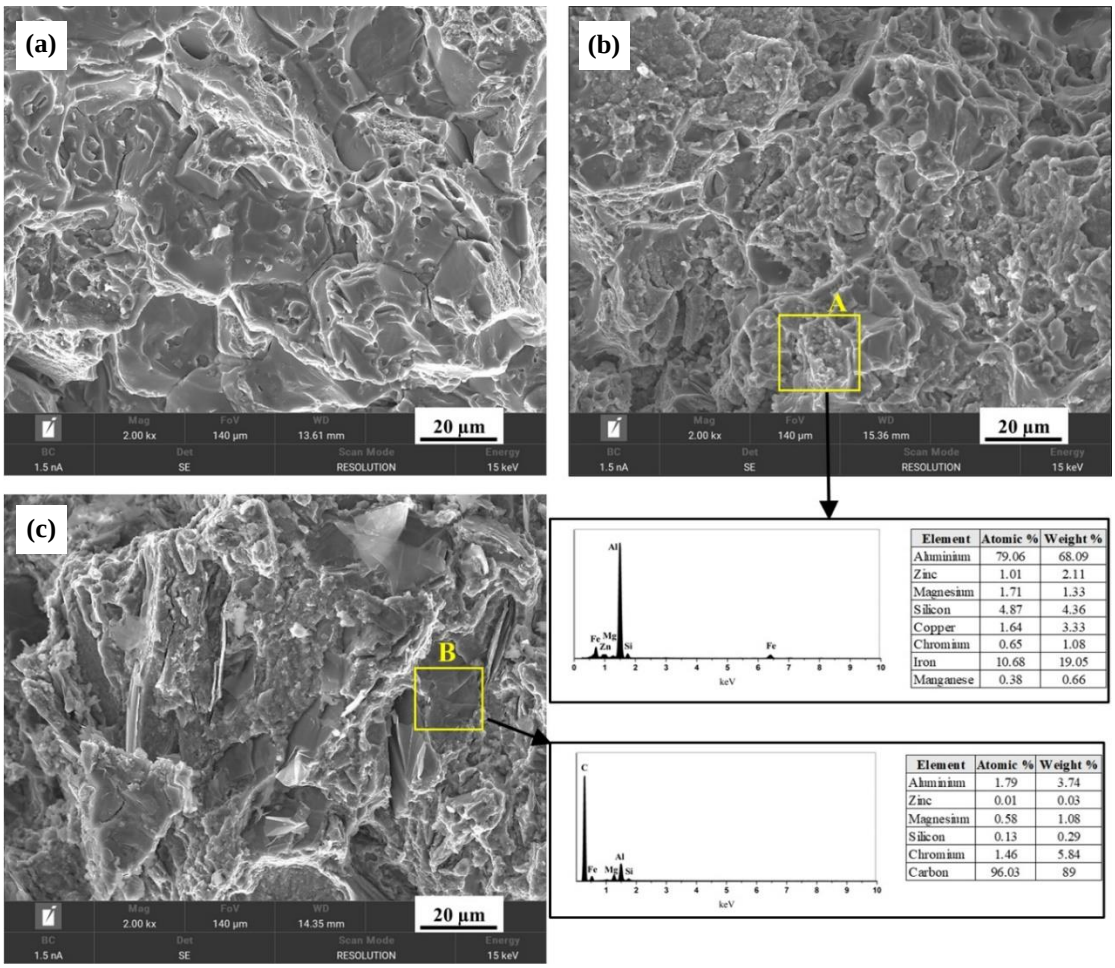

Figure 9 Tensile fracture surfaces along with EDS analysis for (a) Al7075, (b) Al7075/SiC, and (c) Al7075/SiC /Gr under T6 heat treatment.

3.2.4 Tribological behavior

Figure 10 illustrates the variation in weight loss among the fabricated samples after T6 condition. The unreinforced Al7075 alloy exhibited the highest wear loss value of 0.0044. In contrast, the Al7075 alloy reinforced with 1.0 wt.% SiC demonstrated the lowest wear loss, which was approximately 16% lower than that of the unreinforced counterpart. This enhancement in wear resistance is primarily attributed to the increased hardness of nanocomposite relative to the base alloy. In accordance with the Archard equation, the dry sliding wear resistance of a material is directly proportional to its hardness [33].

$$V = \frac{KWS}{3H} \tag{1}$$

Where V denotes the volume loss due to wear, K represents the wear coefficient representing the severity or intensity of wear, S designates the sliding distance, and H denotes to the hardness of the material.

Comparable findings have been reported in previous studies [11, 34]. Furthermore, it was observed that the monolithic Al7075 alloy exhibited the highest coefficient of friction, measured at 0.551. The incorporation of 1.0 wt.% SiC into the Al7075 matrix resulted in a reduction of the coefficient of friction to 0.501, representing an approximate 9% decrease. These observations are in agreement with earlier reports in the literature [35]. The reduction in the coefficient of friction following the incorporation of SiC nanoparticles can be attributed to their ability to impede plastic deformation on the wear surface layer [36]. During sliding, the development of cracks and interfacial flaws may lead to the detachment of SiC particles from the matrix due to diminished adhesion. These dislodged particles act as hard abrasives, contributing to the resistance against material loss through wear. Moreover, the presence of SiC nanoparticles leads to a decrease in the real contact area between the pin and the composite disc, thereby further reducing the coefficient of friction [37]. Bharat and Bose [38] similarly reported that nanoparticles assist in supporting the applied load at the interface between the pin and the counter face, which contributes to lowering the friction coefficient and mitigating surface damage such as scratches and cuts.

However, it was observed that the incorporation of hybrid reinforcements SiC and graphite (Gr) into the Al7075 alloy resulted in a slight increase in both weight loss and the coefficient of friction. This behavior is primarily attributed to the presence of Gr particles, which tend to reduce the hardness and tensile strength of the hybrid composites. While the inclusion of Gr contributes to enhanced lubrication at the wear interface, potentially improving wear resistance, the relatively large particle size of Gr may promote void formation and crack propagation under sliding conditions. These adverse effects are likely due to particle agglomeration and weak interfacial bonding between Al7075/Gr and SiC/Gr. As a result, the overall wear resistance of the Al7075/Gr/SiC hybrid composites was diminished, as evidenced in the present study. Therefore, the optimization of Gr particle size and content is essential for enhancing the wear performance of aluminium-based hybrid composites.

SEM micrographs of the dry sliding worn surfaces of the samples are presented in Figure 11. As depicted in Figure 11(a), the unreinforced Al7075 alloy exhibited pronounced plastic deformation, characterized by the presence of wide and deep grooves, indicative of severe adhesive wear. In contrast, the worn surface of the Al7075/1.0 wt.% SiC nanocomposite, shown in Figure 11(b), revealed narrower grooves and a reduction in the overall number of grooves. This improvement in surface smoothness is attributed to the load-bearing capability of the nano-sized SiC particles, which effectively minimized plastic deformation and facilitated the formation of a lubricating film on the composite surface [39]. Additionally, the worn surface of the hybrid Al7075/SiC/Gr nanocomposite, illustrated in Figure 11(c), appeared rougher than that of the Al7075/1.0 wt.% SiC nanocomposite. This increased roughness is likely due to the detachment of agglomerated Gr particles from the matrix, which adversely affected the surface integrity under sliding conditions.

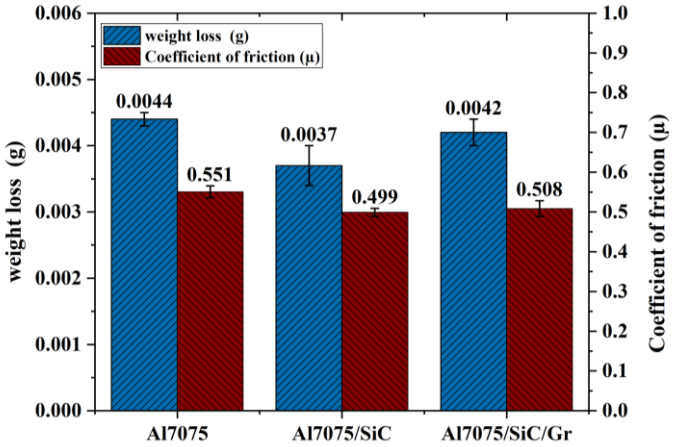

Figure 10 Representative weight loss and coefficient of friction for all fabricated samples.

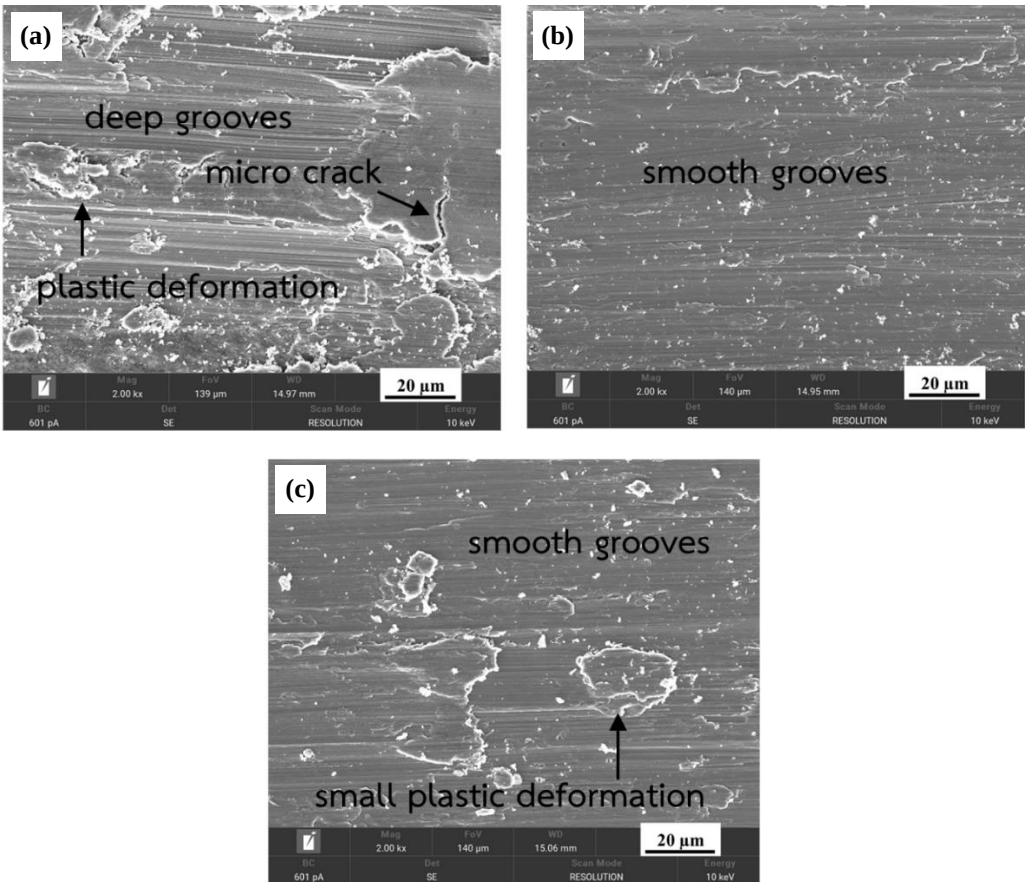

Figure 11 Worn surface of (a) Al7075, (b) Al7075/SiC, (c) Al7075/SiC/Gr, and (d) EDS of square area in (b).

3.2.5 Limitations and potential applications of the findings

This study demonstrated that integrating mechanical alloying-assisted semisolid stir casting, die casting, and T6 treatment can effectively enhance the microstructure and properties of Al7075/SiC composites. However, limitations remain, including 1) Graphite dispersion: Poor wettability and agglomeration of graphite reduced mechanical performance and increased porosity. 2) Statistical robustness: Additional mechanical and tribological testing with larger sample sizes and statistical analyses are needed to confirm the

trends. 3) Processing control: Optimization of parameters such as stirring speed, temperature, and SiC/Gr content is essential to enhance reproducibility and consistency. Therefore, future Directions to overcome the limitation are investigating alternative reinforcement morphologies or surface treatments to improve graphite dispersion. As well as exploring hybrid reinforcement systems with controlled particle size and shape distributions.

The potential for this research finding to benefit a variety of applications, including the aerospace, automotive, and defense industries, where wear resistance and mechanical performance are critical, including lightweight and high-strength materials.

4. Conclusions

This study successfully demonstrated the fabrication and characterization of Al7075-based nanocomposites reinforced with SiC nanoparticles and graphite (Gr) using an integration of mechanical alloying and die casting assisted by T6 heat treatment. Incorporating SiC and Gr substantially influenced the microstructural evolution, mechanical performance, as well as tribological behavior of the composites. Die casting led to substantial grain refinement and reduced porosity, while the application of T6 heat treatment further enhanced microstructural uniformity through dissolution of intermetallic phases and precipitation of strengthening particles. The incorporation of 1.0 wt.% SiC nanoparticles notably improved hardness, tensile strength, and wear resistance, owing to multiple strengthening mechanisms including grain refinement, Orowan looping, dislocation hardening, and effective load transfer. The Al7075/SiC-T6 composite exhibited the highest mechanical performance, achieving a 0.2% proof stress of 250 MPa, an ultimate tensile strength of 364 MPa, and 16% elongation. Although the addition of graphite improved lubrication and reduced the coefficient of friction at higher sliding distances, it resulted in lower hardness and tensile strength due to its inherent brittleness, agglomeration tendencies, and poor wettability with the aluminium matrix. The Al7075/SiC/Gr hybrid composite displayed a mixed fracture mode and showed inferior mechanical and wear performance compared to the SiC-only reinforced counterpart, highlighting the need for optimization of graphite particle size and distribution. Overall, the combination of nano-SiC reinforcement and T6 heat treatment proved to be an effective strategy for significantly enhancing the structural integrity and functional performance of Al7075 composites, making them promising candidates for lightweight, high-performance engineering applications where improved wear resistance and mechanical strength are critical.

5. Acknowledgments

This work was supported by Research of Khon Kaen University.

6. References

[1] Singh K, Singh H, Vardhan S, Mohan S. Mechanical study of Al 7050 and Al 7075 based metal matrix composites: a review. Mater Today: Proc. 2021;43:673-7.
[2] Potisawang C, Talangkun S. Effect of die pressure and injection speed on rheo-die casting of A356-sic composite. Mater Sci Forum. 2019;947:190-4.
[3] Shin S, Park H, Park B, Lee SB, Lee SK, Kim Y, et al. Dispersion mechanism and mechanical properties of SiC reinforcement in aluminium matrix composite through stir-and die-casting processes. Appl Sci. 2021;11(3):952.
[4] Sahoo BP, Das D. Investigation on reinforcement incorporation factor and microstructure of Al 7075/submicron-TiB_2 metal matrix composites processed through a modified liquid metallurgy technique. Exp Tech. 2021;45(2):179-93.
[5] Pedersen KO, Børvik T, Hopperstad OS. Fracture mechanisms of aluminium alloy AA7075-T651 under various loading conditions. Mater Des. 2011;32(1):97-107.
[6] Mobarhan Bonab MA, Simchi A. Effect of silicon carbide nanoparticles on hot deformation of ultrafine-grained aluminium nanocomposites prepared by hot powder extrusion process. Powder Metall. 2016;59(4):262-70.
[7] Law E, Pang SD, Quek ST. Discrete dislocation analysis of the mechanical response of silicon carbide reinforced aluminium nanocomposites. Compos B: Eng. 2011;42(1):92-8.
[8] Ponhan K, Weston D, Tassenberg K. Influence of SiC nanoparticle contents on microstructural evolution and mechanical behavior of AZ91D magnesium matrix composites synthesised through a combination of a master pellet feeding technique and stir casting assisted by ultrasonic vibration. Mater Today Commun. 2023;36:106785.
[9] Shi X, Nie K, Deng K, Xu C. Effect of micro-nano hybrid SiCp on microstructure and mechanical properties of 7075Al alloy. J Mater Res Technol. 2024;32:3476-89.
[10] Taherzadeh Mousavian R, Azari Khosroshahi R, Yazdani S, Brabazon D, Boostani AF. Fabrication of aluminum matrix composites reinforced with nano- to micrometer-sized SiC particles. Mater Des. 2016;89:58-70.
[11] Prakash KS, Balasundar P, Nagaraja S, Gopal PM, Kavimani V. Mechanical and wear behaviour of Mg–SiC–Gr hybrid composites. J Magnes Alloy. 2016;4(3):197-206.
[12] Azimi A, Shokuhfar A, Nejadseyfi O. Mechanically alloyed Al7075–TiC nanocomposite: Powder processing, consolidation and mechanical strength. Mater Des (1980-2015). 2015;66:137-41.
[13] Potisawang C, Talangkun S, Ponhan K. Improvement of microstructure and mechanical properties for Al7075 aluminium reinforced with hybrid graphite and SiC particles via a combination of mechanical alloying and stir casting. Mater Res Express. 2025;12(1):016509.
[14] Ponhan K, Jiandon P, Juntaracena K, Potisawang C, Kongpuang M. Enhanced microstructures, mechanical properties, and machinability of high performance ADC12/SiC composites fabricated through the integration of a master pellet feeding approach and ultrasonication-assisted stir casting. Results Eng. 2024;24:102937.
[15] Ma GN, Wang D, Liu ZY, Xiao BL, Ma ZY. An investigation on particle weakening in T6-treated SiC/Al–Zn–Mg–Cu composites. Mater Charact. 2019;158:109966.
[16] Walde C, Tsaknopoulos K, Champagne V, Cote D. Phase transformations in thermally treated gas-atomized Al 7075 powder. Metallogr Microstruct Anal. 2020;9:419-27.
[17] Saberi Y, Zebarjad SM, Akbari GH. On the role of nano-size SiC on lattice strain and grain size of Al/SiC nanocomposite. J Alloys Compd. 2009;484(1-2):637-40.

[18] Akbarpour MR, Salahi E, Hesari FA, Kim HS, Simchi A. Effect of nanoparticle content on the microstructural and mechanical properties of nano-SiC dispersed bulk ultrafine-grained Cu matrix composites. Mater Des (1980-2015). 2013;52:881-7.
[19] Dong X, Youssef H, Zhnang Y, Wang S, Ji S. High performance Al/TiB_2 composites fabricated by nanoparticle reinforcement and cutting-edge super vacuum assisted die casting process. Compos B: Eng. 2019;177:107453.
[20] Mahathaninwong N, Plookphol T, Wannasin J, Wisutmethangoon S. T6 heat treatment of rheocasting 7075 Al alloy. Mater Sci Eng: A. 2012;532:91-9.
[21] Miranda-López A, León-Patiño CA, Aguilar-Reyes EA, Bedolla-Becerril E, Rodriguez-Ortiz G. Effect of graphite addition on wear behaviour of hybrid Cu/TiC-Gr infiltrated composites. Wear. 2021;484-485:203793.
[22] Madhusudan BM, Ghanaraja S, Sudhakar GN. Synthesis and development of size hybrid nano SiC-Al7075 composites by advanced stir casting. Mater Today: Proc. 2021;43:3804-9.
[23] Xie Y, Huang Y, Wang F, Meng X, Li J, Dong Z, et al. Deformation-driven metallurgy of SiC nanoparticle reinforced aluminium matrix nanocomposites. J Alloys Compd. 2020;823:153741.
[24] Pu B, Lin X, Li B, Chen X, He C, Zhao N. Effect of SiC nanoparticles on the precipitation behavior and mechanical properties of 7075Al alloy. J Mater Sci. 2020;55:6145-60.
[25] Panigrahi SK, Jayaganthan R. Effect of ageing on microstructure and mechanical properties of bulk, cryorolled, and room temperature rolled Al 7075 alloy. J Alloys Compd. 2011;509(40):9609-16.
[26] Tang XC, Meng LY, Zhan JM, Jian WR, Li WH, Yao XH, et al. Strengthening effects of encapsulating graphene in SiC particle-reinforced Al-matrix composites. Comput Mater Sci. 2018;153:275-81.
[27] Boostani AF, Tahamtan S, Jiang ZY, Wei D, Yazdani S, Khosroshahi RA, et al. Enhanced tensile properties of aluminium matrix composites reinforced with graphene encapsulated SiC nanoparticles. Compos A: Appl Sci Manuf. 2015;68:155-63.
[28] Ghiaasiaan R, Amirkhiz BS, Shankar S. Quantitative metallography of precipitating and secondary phases after strengthening treatment of net shaped casting of Al-Zn-Mg-Cu (7000) alloys. Mater Sci Eng: A. 2017;698:206-17.
[29] Wu C, Ma K, Zhang D, Wu J, Xiong S, Luo G, et al. Precipitation phenomena in Al-Zn-Mg alloy matrix composites reinforced with B_4C particles. Sci Rep. 2017;7(1):9589.
[30] Canakci A, Arslan F, Varol T. Physical and mechanical properties of stir-casting processed AA2024/B_4Cp composites. Sci Eng Compos Mater. 2014;21(4):505-15.
[31] Guo H, Yang X, Hu B, Zhu G. Rheo-diecasting process for semi-solid aluminum alloys. J Wuhan Univ Technol-Mat Sci Edit. 2007;22(4):590-5.
[32] Tan C, Zou J, Wang D, Ma W, Zhou K. Duplex strengthening via SiC addition and in-situ precipitation in additively manufactured composite materials. Compos B: Eng. 2022;236:109820.
[33] Manivannan I, Ranganathan S, Gopalakannan S, Suresh S. Mechanical properties and tribological behavior of Al6061–SiC–Gr self-lubricating hybrid nanocomposites. Trans Indian Inst Met. 2018;71:1897-911.
[34] Mosleh-Shirazi S, Akhlaghi F, Li DY. Effect of SiC content on dry sliding wear, corrosion and corrosive wear of Al/SiC nanocomposites. Trans Nonferrous Met Soc China. 2016;26(7):1801-8.
[35] Manivannan I, Ranganathan S, Gopalakannan S, Suresh S, Nagakarthigan K, Jubendradass R. Tribological and surface behavior of silicon carbide reinforced aluminium matrix nanocomposite. Surf Interfaces. 2017;8:127-36.
[36] Cui C, Cui X, Li X, Luo K, Lu J, Ren X, et al. Plastic-deformation-driven SiC nanoparticle implantation in an Al surface by laser shock wave: mechanical properties, microstructure characteristics, and synergistic strengthening mechanisms. Int J Plast. 2018;102:83-100.
[37] Singhal V, Shelly D, Saxena A, Gupta R, Verma VK, Jain A. Study of the influence of nanoparticle reinforcement on the mechanical and tribological performance of aluminum matrix composites—a review. Lubricants. 2025;13(2):93.
[38] Bharat N, Bose PS. Optimizing the wear behaviour of AA7178 metal matrix composites reinforced with SiC and TiO_2 nanoparticles: a comparative study using evolutionary and statistical methods. Silicon. 2023;15(11):4703-19.
[39] Arunkumar T, Pavanan V, Murugesan VA, Mohanavel V, Ramachandran K. Influence of nanoparticles reinforcements on aluminium 6061 alloys fabricated via novel ultrasonic aided rheo-squeeze casting method. Met Mater Int. 2022;28(1):145-54.